Mechanism of the Oxadi-π-methane and [1,3]-Acyl Sigmatropic Rearrangements of β,γ-Enones: A Theoretical Study

Sarah Wilsey,[†] Michael J. Bearpark,[†] Fernando Bernardi,[‡] Massimo Olivucci,*[,‡] and Michael A. Robb*[,†]

Contribution from the Department of Chemistry, King's College London, Strand, London WC2R 2LS, U.K., and Dipartimento di Chimica "G. Ciamician" dell'Universita di Bologna, Via Selmi 2, 40126 Bologna, Italy

Received July 12, 1995[⊗]

Abstract: The oxadi-π-methane ([1,2]-acyl shift) and [1,3]-acyl shift rearrangements of a simple β,γ-enone (but-3-enal) have been investigated using MC-SCF computations in a 6-31G* basis set. The excited state reaction pathways and decay funnels for this model compound can be used to explain the direct and triplet-sensitized photochemistry of β,γ-enones in general. Our calculations show that the "classical" biradical intermediates proposed for both reactions correspond to decay funnels at which *four* states ($S_1(n\pi^*)$, $T_1(\pi\pi^*)$, $T_2(n\pi^*)$, and S_0) are degenerate. Both efficient internal conversion (IC) and efficient intersystem crossing (ISC) can occur at these points, and the ground state reaction path is therefore the same regardless of the state initially populated. The ratio of products formed on photolysis is governed by the relative heights of the barriers leading to these decay funnels, and these will be sensitive to substituent effects on the reactant molecule. The oxadi-π-methane rearrangement is found to occur via a three-step process, where the four-level decay funnel corresponds to the first of two floppy intermediates on S_0. There are two possible mechanisms leading to the [1,3]-acyl shift product: one involving the four-level decay funnel which corresponds to a "tight" intermediate in a quasi-concerted pathway, and a second which involves dissociation and recombination.

Introduction

Photochemical [1,2]- and [1,3]-acyl sigmatropic shifts of β,γ-enones (Scheme 1) represent an important class of reactions which are often used synthetically[1] to carry out skeletal transformations in natural product synthesis. The [1,2]-acyl shift is commonly known as the oxadi-π-methane (ODPM) rearrangement since it is structurally analogous to the di-π-methane rearrangement.[2]

In a recent study, we have been able to document the reaction path for the singlet di-π-methane rearrangement[3] in 1,4-pentadiene. However, the replacement of the C═C bond with a C═O bond enriches the photochemistry dramatically because of the role played by the triplet manifold. As we have recently demonstrated,[4] the mechanism of radiationless decay via the singlet and triplet manifolds in bifunctional compounds such as the conjugated α,β-enone acrolein is very complex in comparison with butadiene.[5] Therefore, the mechanisms of the photochemical sigmatropic isomerization reactions of β,γ-enones require a careful consideration of the type of electronic state ($n\pi^*$ or $\pi\pi^*$) involved together with the change in spin multiplicity that occurs along the reaction coordinate.

The experimental results are very varied. Direct irradiation of β,γ-enones yields mainly the [1,3]-acyl shift product, and

Scheme 1

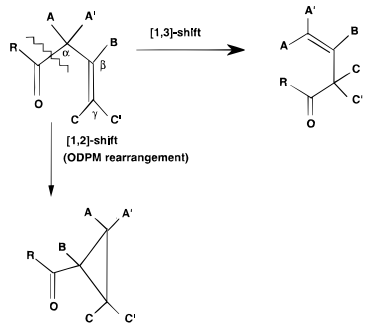

triplet sensitization yields mainly the ODPM product,[6,7] a difference that is often exploited synthetically. However, this selectivity is not universal, and the reasons for this are not fully understood. In some cases the [1,3]-acyl shift product is also formed on triplet sensitization, while the ODPM rearrangement product has been observed on direct photolysis of certain enones.[8−10] Nowadays it is generally accepted that the [1,3]-acyl shift occurs from an $n\pi^*$ excited state in either the singlet (S_1) or triplet (T_2) manifold, while the ODPM rearrangement originates from the slightly lower energy triplet $\pi\pi^*$ state (T_1) where the excitation is localized on the alkene moiety.[11,12] The

[†] King's College London.
[‡] Universita di Bologna.
[⊗] Abstract published in *Advance ACS Abstracts,* December 1, 1995.

(1) See, for example: (a) Singh, V.; Porinchu, M. *J. Chem. Soc., Chem. Commun.* **1993**, 134. (b) Mehta, G.; Subrahmanyam, D. *J. Chem. Soc., Perkin Trans. 1* **1993**, 395. (c) Uyehara, T; Furuta, T.; Akamatsu, M.; Kato, T.; Yamamoto, Y. *J. Org. Chem.* **1989**, *54*, 5411.
(2) Dauben, W. G.; Kellogg, M. S.; Seeman, J. I.; Spitzer, W. A. *J. Am. Chem. Soc.* **1970**, *92*, 1786.
(3) Reguero, M.; Bernardi, F.; Jones, H.; Olivucci, M.; Robb, M. A. *J. Am. Chem. Soc.* **1993**, *115*, 2073.
(4) Reguero, M.; Olivucci, M.; Bernardi, F.; Robb, M. A. *J. Am. Chem. Soc.* **1994**, *116*, 2103.
(5) Olivucci, M.; Ragazos, I. N.; Bernardi, F.; Robb, M. A. *J. Am. Chem. Soc.* **1993**, *115*, 3710.
(6) Büchi, G.; Burgess, E. M. *J. Am. Chem. Soc.* **1960**, *82*, 4333.
(7) Schuster, D. I.; Axelrod, M.; Auerbach, J. *Tetrahedron Lett.* **1963**, 1911.
(8) Schuster, D. I.; Sussman, D. H. *Tetrahedron Lett.* **1970**, 1661.
(9) Engel, P. S.; Schexnayder, M. A.; Ziffler, H.; Seeman, J. I. *J. Am. Chem. Soc.* **1974**, *96*, 924.
(10) (a) Engel, P. S.; Schexnayder, M. A. *J. Am. Chem. Soc.* **1975**, *97*, 145. (b) Engel, P. S.; Schexnayder, M. A. *J. Am. Chem. Soc.* **1972**, *94*, 2252.
(11) (a) Schaffner, K. *Tetrahedron* **1976**, *32*, 641. (b) Mirbach, M. J., Henne, A., Schaffner, K. *J. Am. Chem. Soc.* **1978**, *100*, 7127. (c) Henne, A., Siew, N. P. Y., Schaffner, K. *J. Am. Chem. Soc.* **1979**, *101*, 3671. (d) Henne, A., Siew, N. P. Y., Schaffner, K. *Helv. Chim. Acta* **1979**, *62*, 1952.

0002-7863/96/1518-0176$12.00/0

Scheme 2

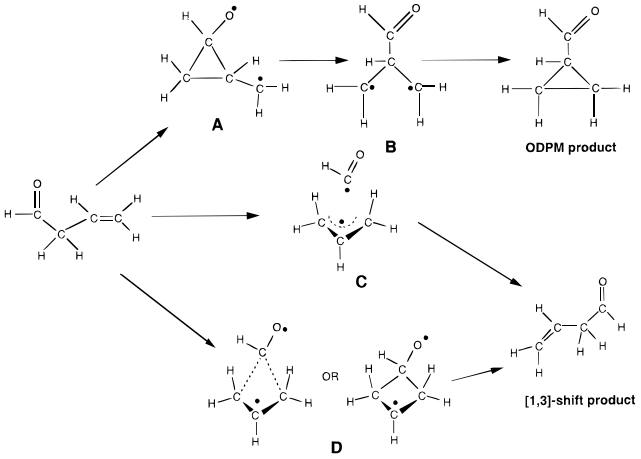

energy difference between the two triplet states is thought to be as little as 2 kcal mol^{-1}.[13] Both rearrangements have been the subject of several reviews,[12a,14,15] and the possible reaction mechanisms have been summarized in Scheme 2.

The ODPM reaction path is proposed to involve the two biradical intermediates **A** and **B**, with **A** being the primary photoproduct and **B** being a short-lived 1,3-biradical which rapidly produces the final three-membered ring product. In contrast, the [1,3]-acyl shift has been proposed to occur via two competitive routes. The first route involves a single intermediate stage corresponding to the formation of a free radical pair, **C**, which recombines to form the final product (i.e., a fragmentation−recombination mechanism). The second route is a quasi-concerted process involving the formation of the four-membered ring biradical intermediate **D**. The intermediate **D** can be either a "tight" intermediate where all the C−C bonds are fully formed or a "loose" intermediate which could be a radical pair held together in a solvent cage. In this case the reaction pathways via **C** and **D** will be two extremes of the same mechanism, and this has lead to problems in determining exactly how the [1,3]-shift product is formed. The actual existence of the species **A**−**D** and the multiplicity of the surfaces on which they are formed have never been demonstrated directly, and therefore it is useful to briefly review the experimental results which support their existence. These are based on three separate observations: (i) the stereochemistry of the reactions, (ii) CIDNP (chemically induced dynamic nuclear polarization) and radical trapping experiments, and (iii) fluorescence and quantum yield measurements.

(i) Reaction Stereochemistry. The ODPM rearrangement is found to occur with a loss in stereochemistry at the α and γ carbon atoms, and on the basis of this stereochemical behavior the existence of the two biradical intermediates **A** and **B** was proposed by both Van de Weerdt et al.[16] and Schaffner et al.[17] These floppy intermediates will give rise to complete scrambling of the substituent groups at the α and γ carbon atoms (Chart 1), provided they have a discrete lifetime. In the few cases where the ODPM rearrangement has been found to be completely stereospecific,[18−20] suggesting a concerted mechanism, the stereospecificity has been put down to steric hindrance.

Chart 1

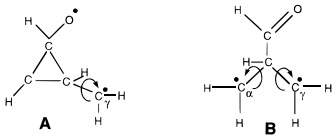

Likewise a loss in stereochemistry[21] is normally observed for the [1,3]-acyl shift reaction, but in this case a dissociation and recombination process via the free radical pair **C** is thought to predominate. The existence of this process has been confirmed by the formation of side products[22] that result from the recombination of free radicals which are sometimes observed on the photolysis of acyclic β,γ-enones and electron-poor olefins. However, in the case of some cyclic β,γ-enones, for example, cyclopentenyl methyl ketones (CPMK), the stereochemistry of the products indicates that the reaction appears to take place at least partly by a quasi-concerted mechanism involving the biradical **D**,[11,23] where no scrambling of the substituent groups on the α and γ carbon atoms would be possible.

(ii) CIDNP and Radical Trapping Experiments. Photo-CIDNP and radical-trapping experiments[11,23] were carried out on CPMK to investigate the mechanisms of both reactions. These molecules were used since they are known[10] to give mainly [1,3]-acyl shift product on direct photolysis and mainly ODPM product on triplet sensitization. They reinforced the idea that on direct photolysis the [1,3]-acyl shift proceeds via a dissociation and recombination mechanism predominantly (i.e., via **C** in Scheme 2). A polarization of the spin multiplicity of the free radical pairs with temperature was observed: at low temperatures triplet radical pairs are produced, while higher temperatures yielded singlet radical pairs. This was assumed to be the result of populating the triplet state nπ^* (T_2) via ISC from the S_1 state at low temperatures, and activating the dissociation process from S_1 at higher temperatures.

(iii) Fluorescence Lifetimes and Quantum Yields. Studies of the change in fluorescence lifetime and quantum yields of the photolysis products of CPMK[11,23] with temperature were also carried out. These indicated two processes with different activation energies that could occur from S_1, leading to the [1,3]-acyl shift product. They were assigned to the dissociation process, which dominates the photochemistry of S_1 around room temperature, leading to the formation of radical pairs **C**, and a concerted process which may involve formation of **D**. Further examination of the 'concerted' reaction, using radical scavenging and triplet quenching by NO and O_2,[24] showed that this pathway could account for up to a quarter of the [1,3]-acyl shift product formed in this case. Both processes were thought to compete with fluorescence and with ISC to T_2 and T_1, forming triplet radicals and ODPM product, respectively. The quantum yield of both of these decreased with temperature, although the quantum yield of the [1,3]-acyl shift product increased overall,

(12) (a) Houk, K. N. *Chem. Rev.* **1976**, *76*, 1. (b) Houk, K. N.; Northington, D. J.; Duke, R. E., Jr. *J. Am. Chem. Soc.* **1972**, *94*, 6233.
(13) Engel, P. S.; Schexnayder, M. A.; Phillips, W. V.; Ziffler, H.; Seeman, J. I. *Tetrahedron Lett.* **1975**, 1157.
(14) Schuster, D. I. Photorearrangements of Enones. In *Rearrangements in Ground and Excited States*; de Mayo, P., Ed.; Academic Press: London, 1980, Vol. 3, p 232.
(15) Hixon, S. S.; Mariano, P. S.; Zimmerman, H. E. *Chem. Rev.* **1973**, *73*, 531.
(16) Van der Weerdt, A. J. A.; Cerfontain, H.; Van der Ploeg, J. P. M.; Hollander, J. A. *J. Chem. Soc., Perkin Trans. 2* **1978**, 155.
(17) Domb, S., Schaffner, K. *Helv. Chim. Acta* **1970**, *53*, 677.
(18) (a) Sato, H.; Furutachi, N.; Nakanishi, K. *J. Am. Chem. Soc.* **1972**, *94*, 2150. (b) Sato, H.; Furutachi, N.; Hayashi, J.; Nakadaira, Y. *Tetrahedron* **1973**, *29*, 275.
(19) Seeman, J. I.; Ziffer, H. *Tetrahedron Lett.* **1973**, 4413.
(20) (a) Coffin, R. L.; Givens, R. S.; Carlson, R. G. *J. Am. Chem. Soc.* **1974**, *96*, 7554. (b) Coffin, R. L.; Cox, W. W.; Carlson, R. G.; Givens, R. S. *J. Am. Chem. Soc.* **1979**, *101*, 3261.
(21) Gonzenbach, H.-U.; Schaffner, K.; Blank, B.; Fischer, H. *Helv. Chim. Acta* **1973** *56*, 1741.
(22) Schexnayder, M. A.; Engel, P. S. *J. Am. Chem. Soc.* **1975**, *97*, 4825.
(23) Sadler, D. E.; Wendler, J.; Olbrich, G.; Schaffner, K. *J. Am. Chem. Soc.* **1984**, *106*, 2064.
(24) Reimann, B.; Sadler, D. E.; Schaffner, K. *J. Am. Chem. Soc.* **1986**, *108*, 5527.

indicating the existence of a [1,3]-acyl shift pathway that is only accessed at higher temperatures.

The two ISC processes from S_1 were investigated by examining the heavy atom effects on bicyclo[3.2.1]octan-2-one and its halogen derivatives, but the results were inconclusive.[25] However, subsequent experiments done by Schuster and co-workers using photochemical quenching and sensitization techniques on 3-methyl-3-(1-cyclopentenyl)butan-2-one[26] and irradiating in the presence of xenon did show an apparent increase in the rate of ISC from S_1 to $T_2(n\pi^*)$. However, S_1-T_1 ISC has never been demonstrated directly.

In summary, acyclic enones give [1,3]-acyl shifts via a dissociation−recombination mechanism involving the radical pair **C**. However, in the case of certain cyclic enones, at least part of the [1,3]-acyl shift product can be attributed to a stereospecific process occurring via a quasi-concerted pathway through the biradical intermediate **D**. The ODPM reaction, on the other hand, is thought to occur via the two biradical structures **A** and **B**, which occur as intermediates in a three-step process. A satisfactory explanation as to how or where the photoexcited reactant evolves and produces these intermediates can only be obtained by means of theoretical computations. For instance, although the existence of ISC is assumed to be an integral part of these mechanisms for the triplet-sensitized reactions, Schaffner et al.[24] admit that it is known neither by which mechanism the T_1 and T_2 species return to S_0 nor whether energy transfer or chemical scavenging (or both) are involved in the quenching of these excited states. Thus, the main target of this work is to document the excited state reaction pathways and decay mechanisms for the simplest β,γ-enone but-3-enal. These model computations can then serve as a basis for reinterpreting the available experimental information and assist in the design of new experiments.

Theoretical and Computational Details

A computational investigation of the mechanisms summarized in Scheme 2 involves both the evaluation of the reaction coordinates and energy barriers on the singlet and triplet state surfaces and the location of singlet−singlet crossings (conical intersections[27−30]) and singlet−triplet crossings. However, while the mapping of ground state reaction paths for thermal reactions has become almost routine, the theoretical study of excited state reactivity using quantum chemical computations is still in its infancy. To overcome this problem, we have recently developed and implemented the methodology needed to study the nature of the funnel that controls the radiationless decay process from an upper to a lower electronic state.[31] These methodologies can be applied to locate low-lying real crossings between potential energy surfaces of the same or different spin multiplicities.

All computations were performed using the multiconfiguration self-consistent field (MC-SCF) program distributed in Gaussian '92[32] with a 6-31G* basis set. The CAS active space consisted of eight electrons and seven orbitals: an n orbital on the oxygen atom, the four orbitals involved in the two π systems (i.e., the π and π^* orbitals on the carbonyl and ethylene moieties), and the σ orbitals in the $C_\alpha-C_{CO}$ bond (the bond that is cleaved in both reactions). The active space is illustrated in Chart 2.

Chart 2

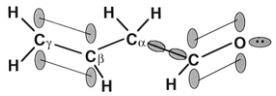

At some geometries this active space has redundant orbitals (i.e., the occupancies are almost exactly 2 or 0). In these cases, the structures were optimized in a smaller active space and single point calculations were then run in the larger active space to obtain comparable energies. In particular, the equilibrium geometries were optimized in an active space of six electrons in five orbitals as the σ orbitals are redundant, while the geometries around the intermediate **B** were optimized in an active space of six electrons in six orbitals as the n orbital was redundant. Numerical frequency and intrinsic reaction coordinate (IRC) calculations were run at the transition states where possible to confirm the nature of the point and the direction of the reaction path followed subsequently. Conical intersection points were characterized using a nonstandard method that has been implemented in a development version of Gaussian.[31c] This method has been used to optimize the conical intersection structures in several papers recently[33] and will not be discussed further. The derivative coupling (DC) and gradient difference (GD) vectors define a branching space in which the degeneracy is lifted at any point along the conical intersection hyperline, and the initial reaction path on the ground state surface must lie in this branching space for very slow nuclear motion (see ref 33i for a discussion of the nature of the reaction path at a conical intersection). These vectors are computed as part of the optimization method. At geometries around the crossing points the degeneracy of the states required us to use state-averaged orbitals.

The singlet−triplet crossing points were computed in the same fashion as the singlet−singlet crossing points, although in this case the crossing space has dimension $n - 1$ since the derivative coupling (DC) is zero. The spin−orbit coupling was computed at these points using a one-electron approximation with the effective charges on O (5.6) and C (3.6) as optimized by Koseki et al.[34]

Results and Discussion

In this section we shall examine the photochemical reaction pathways corresponding to (i) the ODPM rearrangement, (ii) a stereospecific, quasi-concerted [1,3]-acyl shift rearrangement, and (iii) a [1,3]-acyl shift rearrangement based upon a dissociation−recombination mechanism. The discussion of these three reaction pathways (a schematic overview is given in Figures 5−7) will be based on 26 fully optimized structures corresponding to minima, transition states, and real crossing points on the $n\pi^*$ S_1 and T_2 states and on the $\pi\pi^*$ T_1 state. The energetics

(25) Givens, R. S.; Chae, W. K.; Matuszewski, B. *J. Am. Chem. Soc.* **1982**, *104*, 2456.
(26) Schuster, D. I.; Calcaterra, L. T. *J. Am. Chem. Soc.* **1982**, *104*, 6397.
(27) Zimmerman, H. E. *J. Am. Chem. Soc.* **1966**, *88*, 1566.
(28) Michl, J. *J. Mol. Photochem.* **1972**, 243.
(29) Teller, E. *Isr. J. Chem.* **1969**, *7*, 227.
(30) (a) Von Neumann, J.; Wigner, E. *Phys. Z.* **1929**, *30*, 467. (b) Teller, E. *J. Phys. Chem.* **1937**, *41*, 109. (c) Herzberg, G.; Longuet-Higgins, H. C. *Trans. Faraday Soc.* **1963**, *35*, 77. (d) Atchity, G. J.; Xantheas, S. S.; Ruedenberg, K. *J. Chem. Phys.* **1991**, *95*, 1862.
(31) (a) Ragazos, I. N.; Robb, M. A.; Bernardi, F.; Olivucci, M. *Chem. Phys. Lett.* **1992**, *197*, 217. (b) Yarkony, R. D. *J. Phys. Chem.* **1993**, *97*, 4407. (c) Bearpark, M. J.; Robb, M. A.; Schlegel, H. B. *Chem. Phys. Lett.* **1994**, *223*, 269.
(32) Gaussian '92, Revision B: Frisch, M. J.; Trucks, G. W.; Head-Gordon, M.; Gill, P. M. W.; Wong, M. W.; Foresman, J. B.; Johnson, B. G.; Schlegel, H. B.; Robb, M. A.; Replogle, E. S.; Gomperts, R.; Andres, J. L.; Raghavachari, K.; Binkley, J. S.; Gonzalez, C.; Martin, R. L.; Fox, D. J.; Defrees, D. J.; Baker, J.; Stewart, J. J.; Pople, J. A., Gaussian, Inc., Pittsburgh, PA, 1992.
(33) (a) Bernardi, F.; De, S.; Olivucci, M.; Robb, M. A. *J. Am. Chem. Soc.* **1990**, *112*, 1737. (b) Reguero, M.; Bernardi, F.; Bottoni, A.; Olivucci, M.; Robb, M. A. *J. Am. Chem. Soc.* **1991**, *113*, 1566. (c) Bernardi, F.; Ragazos, I. N.; Olivucci, M.; Robb, M. A. *J. Am. Chem. Soc.* **1992**, *114*, 2752. (d) Bernardi, F.; Olivucci, M.; Robb, M. A. *J. Am. Chem. Soc.* **1992**, *114*, 5805. (e) Bernardi, F.; Olivucci, M.; Palmer, I. J.; Robb, M. A. *J. Org. Chem.* **1992**, *57*, 5081. (f) Bernardi, F.; Ragazos, I. N.; Olivucci, M.; Robb, M. A. *J. Am. Chem. Soc.* **1992**, *114*, 8211. (g) Palmer, I. J.; Ragazos, I. N.; Bernardi, F.; Olivucci, M.; Robb, M. A. *J. Am. Chem. Soc.* **1993**, *115*, 673. (h) Bernardi, F.; Olivucci, M.; Robb, M. A. *Isr. J. Chem.* **1993**, *33*, 256. (i) Olivucci, M.; Bernardi, F.; Ragazos, I. N.; Robb, M. A. *J. Am. Chem. Soc.* **1994**, *116* 1077. (j) Bernardi, F.; Bottoni, A.; Olivucci, M.; Venturini, A.; Robb, M. A. *J. Chem. Soc., Faraday Trans.* **1994**, *90*, 1617. (k) Palmer, I. J.; Bernardi, F.; Olivucci, M.; Ragazos, I. N.; Robb, M. A. *J. Am. Chem. Soc.* **1994**, *116*, 2121. (l) Olivucci, M.; Bernardi, F.; Ottani, S.; Robb, M. A. *J. Am. Chem. Soc.* **1994**, *116*, 2034. (m) Yamamoto, N.; Bernardi, F.; Olivucci, M.; Robb, M. A.; Wilsey, S. *J. Am. Chem. Soc.* **1994**, *116*, 2064. (n) Celani, P.; Ottani, S.; Olivucci, M.; Bernardi, F.; Robb, M. A. *J. Am. Chem. Soc.* **1994**, *116*, 10141.
(34) Koseki, S.; Schmidt, M. W.; Gordon, M. S. *J. Phys. Chem.* **1992**, *96*, 10768.

Table 1. Energetics for Reactions from the $^1(n\pi^*)$ Surface[a]

geometry	state	energy relative to S_1 vertical excitation (kcal mol^{-1})
reactant (Figure 1a)	S_0	−108.9
	$^1(n\pi^*)$	0.0
minimum (Figure 1d)	$^1(n\pi^*)$	−20.0[a]
$S_1(n\pi^*)$ ODPM Reaction Path (See Figure 5)		
transition state (Figure 2e)	$^1(n\pi^*)$	−0.7[a]
ODPM conical intersection (Figure 2a)	S_0	−12.1
	$^1(n\pi^*)$	−8.9
minimum (Figure 2b)	S_0	−19.9
conical intersection (Figure 2h)	S_0	−2.4
	$^1(n\pi^*)$	−2.4
transition state (Figure 2k)	S_0	−31.1
biradicaloid minimum (Figure 2i)	S_0	−36.5
ODPM product (Figure 1b)	S_0	−98.0
$S_1(n\pi^*)$ Quasi-Concerted [1,3]-Acyl Shift Reaction Path (see Figure 6)		
transition state (Figure 3e)	$^1(n\pi^*)$	+15.8[a]
[1,3]-shift conical intersection (Figure 3a)	S_0	−15.8
	$^1(n\pi^*)$	−15.6
minimum (Figure 3b)	S_0	−17.6
transition state (Figure 3h)	S_0	−12.7
[1,3]-shift product (Figure 1c)	S_0	−108.9
$S_1(n\pi^*)$ Fragmentation Reaction Path (See Figure 7)		
transition state to fragmentation (Figure 4a)	$^1(n\pi^*)$	−3.4

[a] Structures not accurately optimized since state-averaging had to be used.

Table 2. Energetics for Reactions from the $^3(\pi\pi^*)$ Surface

geometry	state	energy relative to T_1 vertical excitation (kcal mol^{-1})
reactant (Figure 1a)	S_0	−105.9
	$^3(\pi\pi^*)$	0.0
minimum (Figure 1e)	$^3(\pi\pi^*)$	−24.7
$^3(\pi\pi^*)$ ODPM Reaction Path (See Figure 5)		
transition state (Figure 2f)	$^3(\pi\pi^*)$	−7.8
ODPM conical intersection (Figure 2a)	$^3(\pi\pi^*)$	−10.2
minimum (Figure 2c)	$^3(\pi\pi^*)$	−6.1
conical intersection (Figure 2h)	$^3(\pi\pi^*)$	+30.6
transition state (Figure 2j)	$^3(\pi\pi^*)$	−14.6
biradicaloid minimum (Figure 2i)	$^3(\pi\pi^*)$	−35.5
$^3(\pi\pi^*)$ Quasi-Concerted [1,3]-Acyl Shift Reaction Path (See Figure 6)		
transition state (Figure 3f)	$^3(\pi\pi^*)$	−5.7
[1,3]-shift conical intersection (Figure 3a)	$^3(\pi\pi^*)$	−13.4
minimum (Figure 3c)	$^3(\pi\pi^*)$	−13.7

Table 3. Energetics for Reactions from the $^3(n\pi^*)$ Surface

geometry	state	energy relative to T_2 vertical excitation (kcal mol^{-1})
reactant (Figure 1a)	S_0	−109.2
	$^3(n\pi^*)$	0.0
minimum (Figure 1f)	$^3(n\pi^*)$	−27.3
$^3(n\pi^*)$ ODPM Reaction Path (See Figure 5)		
transition state (Figure 2g)	$^3(n\pi^*)$	−7.0
ODPM conical intersection (Figure 2a)	$^3(n\pi^*)$	−8.0
minimum (Figure 2d)	$^3(n\pi^*)$	−19.0
conical intersection (Figure 2h)	$^3(n\pi^*)$	−21.1
$^3(n\pi^*)$ Quasi-Concerted [1,3]-Acyl Shift Reaction Path (See Figure 6)		
transition state (Figure 3g)	$^3(n\pi^*)$	+10.5
[1,3]-shift conical intersection (Figure 3a)	$^3(n\pi^*)$	−15.7
minimum (Figure 3d)	$^3(n\pi^*)$	−16.1
$^3(n\pi^*)$ Fragmentation Reaction Path (See Figure 7)		
transition state to fragmentation (Figure 4b)	$^3(n\pi^*)$	−14.4

are summarized in Tables 1−3. The corresponding optimized molecular structures are given in Figures 1−4.

Direct photolysis must involve either radiationless decay via internal conversion (IC) at a S_1/S_0 conical intersection or S−T decay via intersystem crossing (ISC) through a singlet−triplet crossing. ISC must then be followed by passage through a second $T-S_0$ crossing point where decay to the ground state can occur. Sensitized photolysis must involve efficient ISC from a triplet surface to the ground state. Remarkably, for both the ODPM rearrangement and the stereospecific [1,3]-acyl shift paths, evolution of the initial excited state reactant on the potential energy surface leads to a decay region where the S_1, T_1, T_2, and S_0 states are *all degenerate*. Furthermore, the geometry of the molecule in these regions corresponds to the intermediate **A** (see structures in Figure 2a−d) for the ODPM rearrangement, and to the intermediate **D** (see structures in Figure 3a−d) for the stereospecific [1,3]-acyl shift. As we shall show in this section, the presence of a *four-state* degeneracy at these biradicaloid intermediates **A** and **D**, and a fragmentation process via structure **C**, is crucial for rationalizing the mixture of products formed on both direct and triplet-sensitized photolysis. At these points efficient decay to the ground state surface can occur from the excited state surfaces by IC from S_1 or by ISC from the triplet manifold to S_0. It is important to note that while the structures **A** and **D** can be seen as "funnels" on the singlet excited state, they are real intermediates (i.e., potential energy minima) on the S_0 potential energy surface (see Figures 2b and 3b), although their lifetime is expected to be very short. They are also found to be intermediates on the T_1 (Figures 2c and 3c) and T_2 (Figures 2d and 3d) surfaces.

(i) ODPM Reaction Pathway. A schematic representation of the computed energy profile for the ODPM reaction pathway is shown in Figure 5. As discussed above, the most important mechanistic feature along this profile is the presence of a 4-fold degeneracy which is separated from the excited state reactant (either singlet or triplets) by an energy barrier. This structure corresponds to that of the intermediate **A**, as can be seen by looking at the optimized structures in Figure 2a−d.

The origin of the 4-fold degeneracy can easily be rationalized from the character of the two unpaired electrons in these structures. These two electrons can be considered almost uncoupled, both from each other and from the rest of the molecule, and since the coupling between the two radical centers is so small, the triplet and singlet states must be degenerate. Furthermore, at the oxygen atom one is left with a singly occupied p-orbital and a lone pair located along orthogonal axes in space. The $S_1(n\pi^*)$ and $T_2(n\pi^*)$ states can be derived from the S_0 and T_1 states by swapping the relative occupancies of the singly occupied p-orbital and lone pair. However, this difference will not affect the energy, and therefore all four states (S_1, S_0, T_1, and T_2) will be degenerate. This behavior is consistent with the directions defined by the gradient difference and derivative coupling vectors at the S_0/S_1 crossing point (Figure 2a) which indicate the type of molecular distortion required to split the degeneracy.[31] These vectors correspond to the stretching of either the $C_{CO}-C_\alpha$ or the $C_{CO}-C_\beta$ bond,

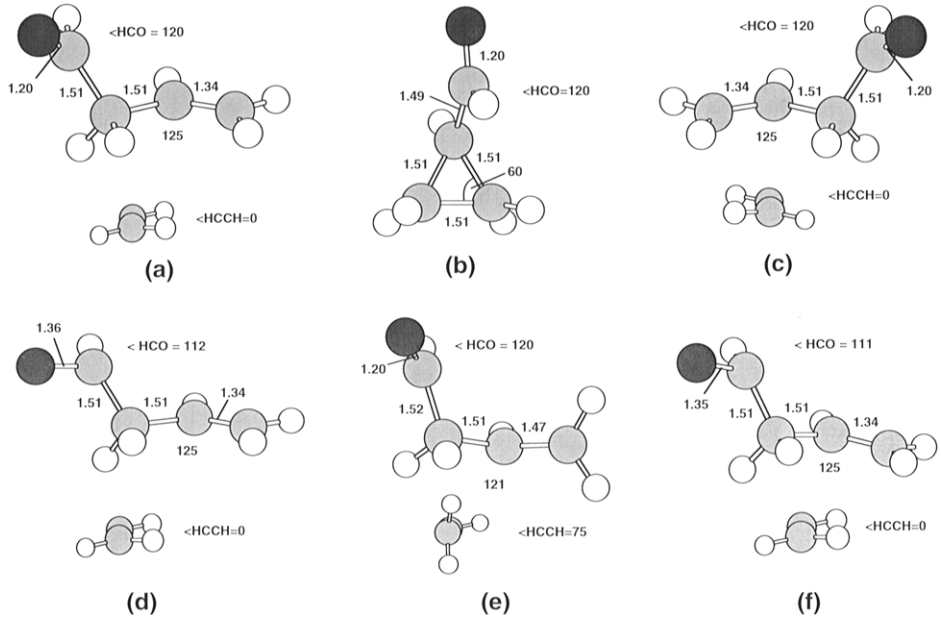

Figure 1. Optimized structures of reactant minima and products (bond lengths in angstroms and angles in degrees): (a) S_0 reactant molecule; (b) ODPM product; (c) [1,3]-shift product (mirror image of reactant molecule); (d) S_1 reactant minimum; (e) T_1 reactant minimum; (f) T_2 reactant minimum.

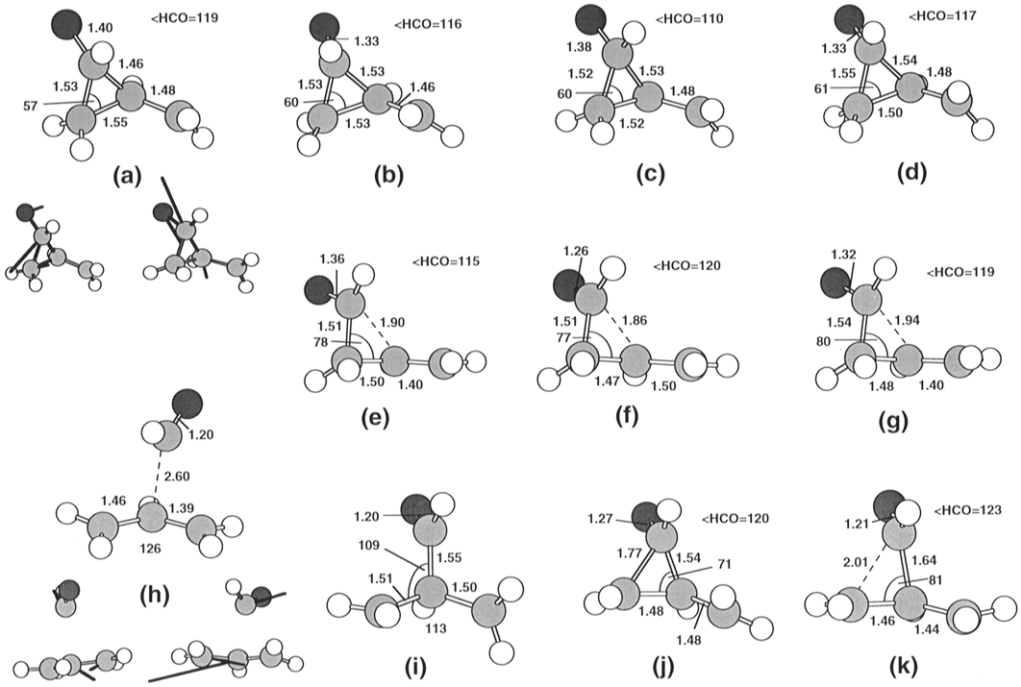

Figure 2. Optimized structures on the ODPM reaction path: (a) ODPM conical intersection (with gradient difference and derivative coupling vectors shown below); (b) minimum adjacent to ODPM conical intersection on S_0; (c) minimum adjacent to ODPM conical intersection on T_1; (d) minimum adjacent to ODPM conical intersection on T_2; (e) reactant minimum—ODPM conical intersection transition state on S_1; (f) reactant minimum—ODPM conical intersection transition state on T_1; (g) reactant minimum—ODPM conical intersection transition state on T_2; (h) di-π-methane-like conical intersection (with gradient difference and derivative coupling vectors shown below); (i) biradical minimum on T_1; (j) ODPM conical intersection—biradical minimum transition state on T_1; (k) ODPM conical intersection—biradical minimum transition state on S_0.

which would both split the degeneracy by increasing the coupling between the two radical centers and the electrons in the two breaking bonds. The spin−orbit coupling computed between singlet and triplet surfaces with different electronic configurations (i.e., $S(n\pi^*)/T(\pi\pi^*)$ and $T(n\pi^*)/S_0$) was found to be large (69 cm^{-1}), but small (11 cm^{-1}) between surfaces with the same electronic configurations. However, the presence of the conical intersection means that decay to the ground state surface will be fully efficient from each of the excited states.

The reaction profile in Figure 5 shows that the accessibility of the decay region for the ODPM reaction is controlled by an excited state barrier. The geometries of the excited state equilibrium structures on the $^1(n\pi^*)$, $^3(\pi\pi^*)$, and $^3(n\pi^*)$ energy surfaces are shown in Figure 1d−f. The S_1 and T_2 minima have pyramidalized carbonyl groups as expected for $n\pi^*$ states. At the minimum on T_1, the carbonyl group is planar but the ethylene group is twisted. The vertical excitation energies for the various states had to be calculated using state-averaged orbitals at the ground state equilibrium geometry (Figure 1a), and for this system the $^3(n\pi^*)$ vertical excitation energy lies about 3 kcal mol^{-1} above that of the $^3(\pi\pi^*)$ which is in acceptable agreement with experiment.[13] Notice that the

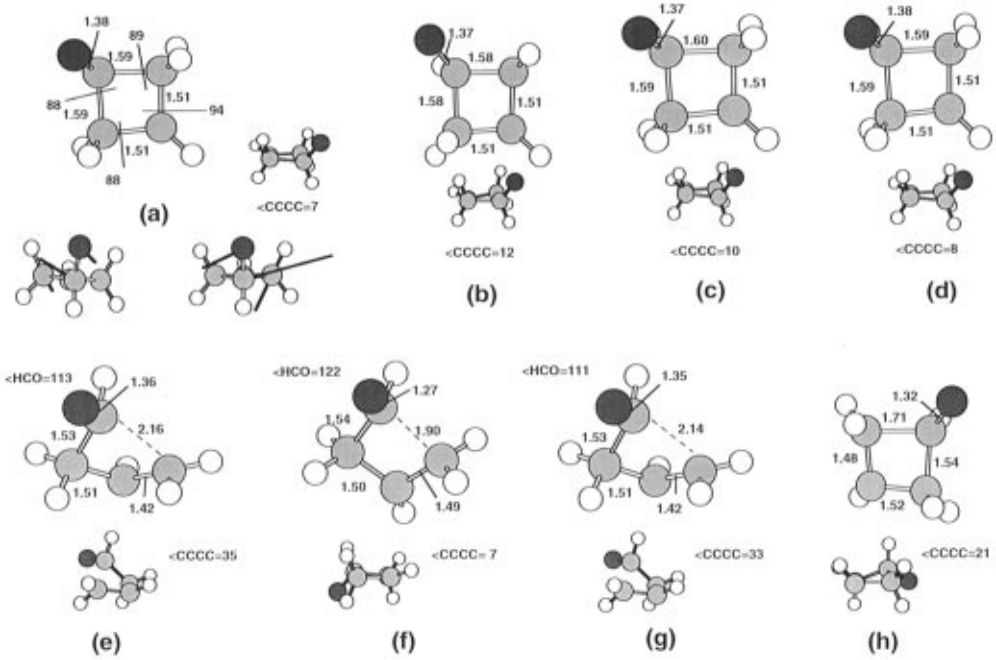

Figure 3. Optimized structures on the quasi-concerted [1,3]-acyl shift reaction path: (a) [1,3]-shift conical intersection (with gradient difference and derivative coupling vectors shown below); (b) minimum adjacent to [1,3]-shift conical intersection on S_0; (c) minimum adjacent to [1,3]-shift conical intersection on T_1; (d) minimum adjacent to [1,3]-shift conical intersection on T_2; (e) reactant minimum−[1,3]-shift conical intersection transition state on S_1; (f) reactant minimum−[1,3]-shift conical intersection transition state on T_1; (g) reactant minimum−[1,3]-shift conical intersection transition state on T_2; (h) [1,3]-shift conical intersection−[1,3]-shift product transition state on S_0.

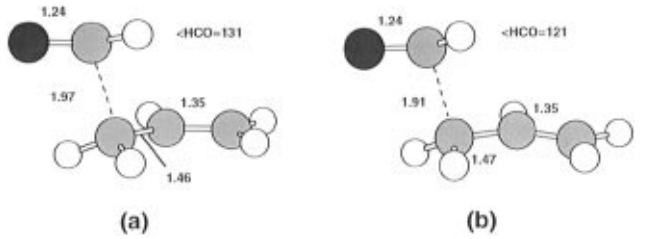

Figure 4. Optimized structures on the fragmentation reaction path: (a) transition state for fragmentation from the S_1 reactant minimum; (b) transition state for fragmentation from the T_2 reactant minimum.

existence of a minimum and a barrier on the $^1(n\pi^*)$ surface close to the vertical excitation energy is consistent with the observed temperature dependence of the fluorescence.[11,23]

The transition states on all three excited state surfaces (Figure 2e−g) leading from the optimized excited state minima (Figure 1d−f) to the decay region have been fully optimized. In each case the energy of the transition state is similar to the energy of the vertically excited state (Tables 1−3) with the minima lying 20 kcal mol^{-1} lower in energy. In fact for our model system, the transition states on $T_2(n\pi^*)$, $T_1(\pi\pi^*)$, and $S_1(n\pi^*)$ lie about 7, 8, and 0.7 kcal mol^{-1} below the vertical excitation energies, respectively.

The singlet and triplet $n\pi^*$ surfaces have similar energies everywhere along the reaction coordinate, and in the transition state region (at geometries where the C═O π bond is broken) the spin−orbit coupling constant is 21 cm^{-1}, indicating that ISC would be possible. The transition state structures on the singlet and triplet $n\pi^*$ surfaces (Figure 2e,g) are very similar whereas the geometry of the transition state on the $^3(\pi\pi^*)$ surface (Figure 2f) has a shorter C═O bond. The $T_1(\pi\pi^*)$ surface is the lowest energy excited state surface at all geometries before the conical intersection region, and it is usually assumed that the majority of ODPM product is formed from this surface on triplet sensitization.

The ground state potential energy surface in the region of the intermediate **A** (i.e., ODPM decay region) is very flat. Consequently optimized geometries in this region are not accurately determined due to the presence of several very small eigenvalues in the Hessian corresponding to methylene torsions. We located a minimum (Figure 2b) on the ground state surface at a geometry that is almost identical to that of the S_1/S_0 conical intersection itself, and in this structure there is free rotation about the $C_\beta-C_\gamma$ bond which is consistent with a loss in stereochemistry at the γ carbon atom (see Chart 1). However, the surface is so flat that we have not been able to fully optimize the structure at this point. An S_0 transition state, adjacent to the conical intersection, was characterized involving partial cleavage of the $C_{CO}-C_\alpha$ bond (Figure 2k), leading to a second biradicaloid minimum (Figure 2i). This minimum corresponds to the second biradical intermediate (**B** in Scheme 2) that has been postulated in the mechanism of this reaction. At this type of geometry free rotation about both the $C_\alpha-C_\beta$ and $C_\beta-C_\gamma$ bonds can occur, and this will lead to the loss in stereochemistry at both the α and γ carbon atoms (see Chart 1) that has been observed experimentally. In this structure, the unpaired electrons on C_α and C_γ can then recouple to form the ODPM product (Figure 1b) with virtually no activation energy. We also located a transition state on T_1 (Figure 2j) at a similar geometry, leading to the biradicaloid minimum. Although we could not fully optimize the intermediate **B** on S_0, it appears that the biradicaloid minimum on T_1 (Figure 2i) has almost the same energy (see Tables 1−3). However, it is doubtful that the molecule will reach this point on the triplet surface as it is more likely to have decayed to S_0 already.

The singlet ODPM reaction will be essentially concerted since decay via the S_1/S_0 conical intersection will occur within one vibrational period and leads to the S_0 intermediate which will immediately rearrange. The mechanism of the triplet reactions involves the same funnel, but since the triplet surfaces have minima at the decay region, the trajectory on these surfaces may carry out many vibrations in these minima before ISC can

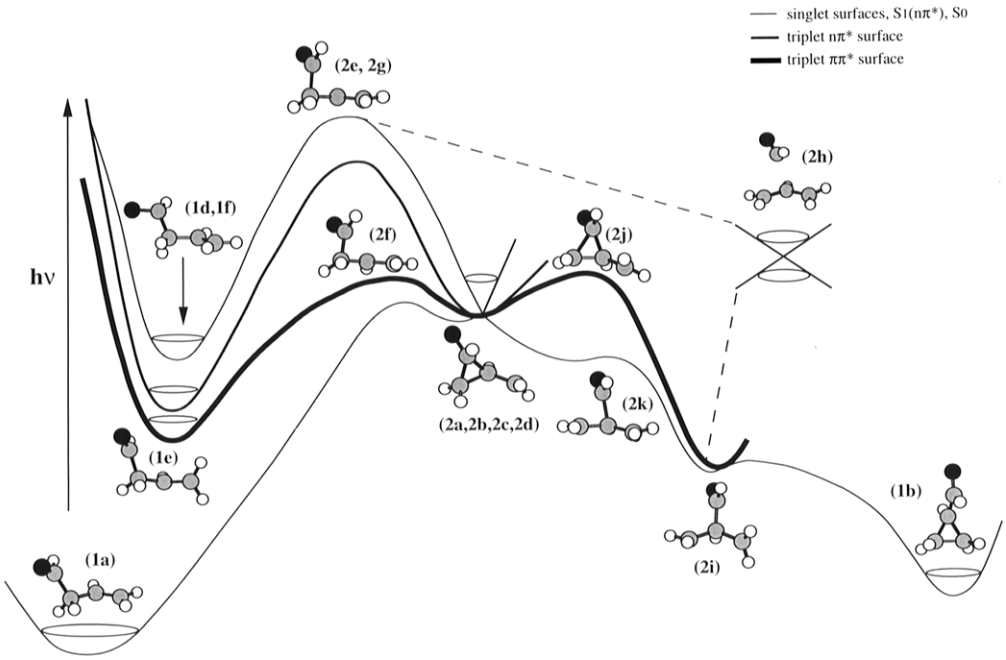

Figure 5. A schematic representation of the potential energy surface for the ODPM reaction.

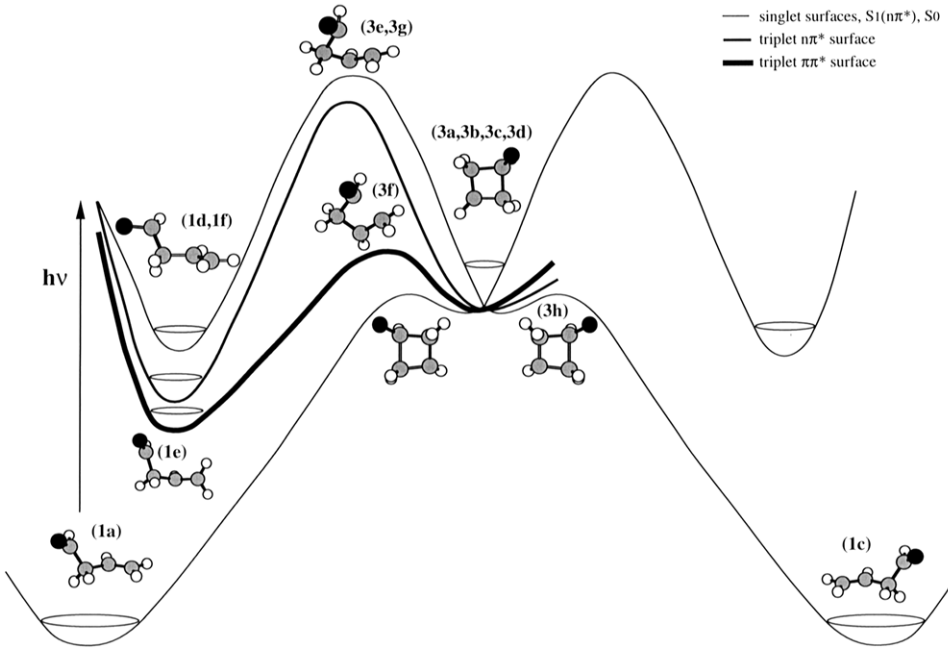

Figure 6. A schematic representation of the potential energy surface for the quasi-concerted [1,3]-shift reaction.

occur. Therefore, we expect the triplet reaction to be stepwise with formation of the triplet biradicaloid intermediate **A** where the stereochemistry of the reactant can be lost. However, the large value of the spin−orbit coupling computed between the T_2 and T_1 states and the singlet surfaces with *different electronic configurations* (69 cm^{-1}) indicates that this decay can be quite efficient.

A distinct conical intersection (Figure 2h) was also located at a geometry almost identical to the one previously reported for the di-π-methane reaction.[3] In contrast to the ODPM conical intersection, the carbonyl bond length is shorter (1.2 Å), and we have four unpaired electrons on four different carbon centers. The degeneracy at this structure has the same origin as in the di-π-methane reaction, and this conical intersection offers an alternative decay point for the singlet reaction.

(ii) [1,3]-Acyl Shift Reaction Pathway. As we have discussed briefly in the introduction to this section, a decay region where the singlet and triplet manifolds are quasi-degenerate also forms the hub of a stereospecific [1,3]-acyl shift reaction pathway, and a sketch of the corresponding energy profile is shown in Figure 6. In our model system, the transition states on the nπ* surfaces lie above the energy of vertical excitation, suggesting that the lower energy path to fragmentation (which we will discuss in the next subsection) can compete effectively. However, in many cyclic systems, the barrier for the nπ* S_1 concerted pathway could be lowered such that this pathway could be populated. For example, the conformation of the five-membered ring in CPMK will reduce the carbonyl carbon and C_γ distance at the S_1 minimum such that this mechanism will be favorable. We will show in this section that on triplet sensitization a quasi-concerted [1,3]-acyl shift reaction can also occur from the $^3(\pi\pi^*)$ surface.

The decay region on the [1,3]-acyl shift reaction path (Figure 3a−d) occurs at a geometry (corresponding to **D** in Scheme 2)

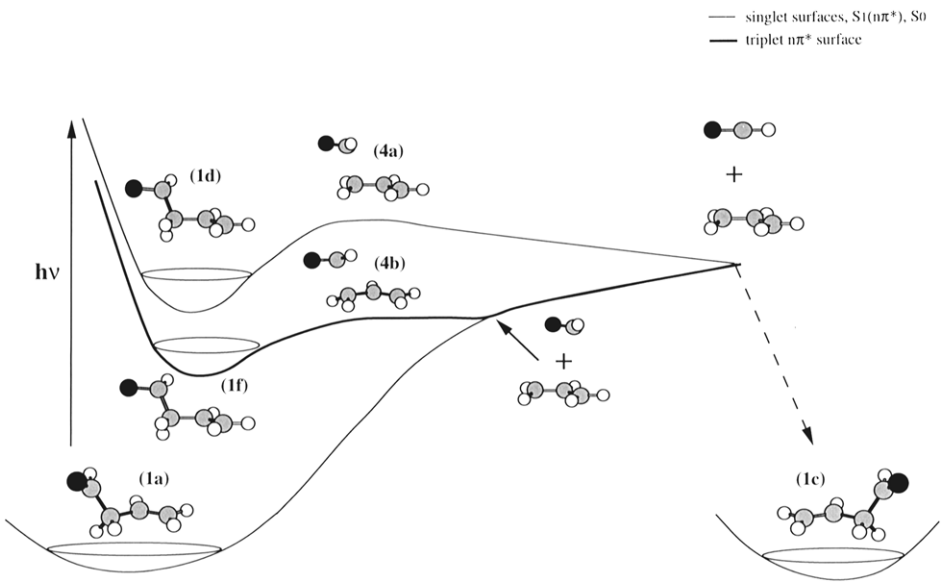

Figure 7. A schematic representation of the potential energy surface for fragmentation.

where there is a four-membered ring of carbon atoms, with unpaired electrons on the oxygen and C_β atoms. The ring is almost planar, and the hydrogen atom attached to the β carbon atom is on the same side of the ring as the oxygen atom such that there is no electronic coupling between the unpaired electrons. At this geometry, the bond between the carbonyl carbon atom and Cγ is fully formed such that there are two possible degenerate configurations of the three electrons in the two orbitals at the oxygen center. Therefore, the four-level degeneracy arises in the same fashion as at the ODPM decay region (structure **A**) discussed in subsection i. Similarly, there is a large computed spin−orbit coupling between triplet and singlet states with *different electronic configurations* at the oxygen atom (63 cm^{-1}) and a smaller value (29 cm^{-1}) for triplet and singlet states with the same electronic configuration at the oxygen atom. Again this interpretation is substantiated by the nature of the gradient difference and derivative coupling vectors for the S_1/S_0 conical intersection (Figure 3a). These vectors indicate that splitting of the degeneracy occurs for a change in the $C_{CO}-C_\alpha$ and $C_{CO}-C_\gamma$ bond lengths.

While the initial motion on the ground state surface following singlet decay must involve bond rupture (as in the ODPM reaction), the gradient on S_0 in the immediate vicinity of the decay point is very small, and there is an adjacent minimum (Figure 3b) corresponding to the intermediate **D**. This intermediate is separated from the [1,3]-acyl shift product by a 5 kcal mol^{-1} barrier (Figure 3h). Similarly, there are real **D**-type intermediates on both the triplet surfaces (Figure 3c,d) in the same region, and therefore ISC from these triplet surfaces will be efficient. As in the case of the ODPM mechanism, the singlet reaction will be quasi-concerted via the S_0/S_1 conical intersection while the triplet reactions, because of the minima at the decay point, may not be concerted. However, the biradicaloid intermediate **D** is very rigid, and therefore any loss in stereochemistry is more likely to be the result of free radical pair formation as we shall show in the next subsection.

The two transition states on the $^1(n\pi^*)$ surface (Figure 3e) and the $^3(n\pi^*)$ surface (Figure 3g) connecting the decay region with the excited state reactant lie 16 and 11 kcal mol^{-1} above the energy of vertical excitation for our model system (the transition state on the singlet surface could only crudely be optimized using state-averaged orbitals). These energetics suggest that the [1,3]-acyl shift product for acyclic β,γ-enones must mainly be formed via the dissociation−recombination mechanism. This agrees with the fact that experimentally these molecules often give side products that can be attributed to free radical recombination reactions.[15] However, in certain cyclic enones (e.g., CPMK[24]) the nπ^* transition states are stabilized so that some of the [1,3]-acyl shift product would be formed via this quasi-concerted, stereospecific mechanism. The transition state on the $^3(\pi\pi^*)$ surface (Figure 3f) was located at an energy 6 kcal mol^{-1} below the vertical excitation energy. The structure has a geometry similar to the analogous barrier on the $^3(n\pi^*)$ surface (Figure 3g) but with the $C_\beta-C_\gamma$ bond stretched (single bond length) and the C−O bond short (double bond length). The $^3(\pi\pi^*)$ barrier for the [1,3]-acyl shift reaction lies 2 kcal mol^{-1} above the $^3(\pi\pi^*)$ barrier, leading to the ODPM conical intersection, and therefore the ODPM and [1,3]-acyl shift reactions may compete on triplet sensitization.

(iii) Dissociation−Recombination Mechanism. A dissociation−recombination mechanism provides another possible route to the [1,3]-acyl shift product. A sketch of the potential energy surface for the pathway leading to dissociation is shown in Figure 7. There is a transition state (Figure 4a) (with a $C_\beta-C_{CO}$ bond length of 1.97 Å) for fragmentation from the $^1(n\pi^*)$ minimum (Figure 1d), which was located about 3 kcal mol^{-1} below the energy of vertical excitation. A similar transition state exists (Figure 4b) on the $^3(n\pi^*)$ state about 14 kcal mol^{-1} below the energy of vertical excitation. Dissociation via these transition states leads to two free radicals (corresponding to structure **C** in Scheme 2), a propenyl radical and a formyl radical. IRCs run from these transition states show that the formyl radical formed from the singlet surface is in its first excited doublet state and can decay to the ground state at a linear geometry where the two surfaces become degenerate. The formyl radical formed from the $^3(n\pi^*)$ surface is already in the lowest energy doublet state. These radicals can then recombine with a propenyl radical to form either the [1,3]-acyl shift product or a reactant molecule.

The fragmentation reaction is one of the temperature-activated processes that has been observed to compete with fluorescence.[11,23] Our results show that the fragmentation barrier on the $^3(n\pi^*)$ triplet surface (Figure 4b) is significantly lower in energy than the energy of the barrier for $^1(n\pi^*)$ fragmentation. This is consistent with the change in the polarization of the [1,3]-acyl shift product with temperature that is sometimes observed.[23,24] On direct photolysis the $^3(n\pi^*)$ surface can be populated (although this will not be efficient) via ISC from S_1

close to the transition state regions such that at low temperatures we can have a fragmentation reaction from the triplet nπ* surface. In the model system studied, the barrier to ^{1}(nπ*) fragmentation is about 2 kcal mol^{-1} lower than the ^{1}(nπ*) ODPM reaction barrier, such that the dissociation−recombination reaction can compete effectively with the ODPM reaction. However, this competition will be sensitive to perturbations introduced by substituent effects.

Conclusions

In this work we have documented the ^{1}(nπ*), ^{3}(nπ*), and ^{3}($\pi\pi$*) reaction paths for the oxadi-π-methane ([1,2]-acyl sigmatropic) and [1,3]-acyl sigmatropic rearrangements for a model β,γ-enone system. Our objective was to investigate computationally the existence and nature of the reaction intermediates **A**−**D** which were proposed on the basis of the experimental evidence (see Tables 1−3 and Scheme 2). Our computations indicate that the mechanistically relevant structures controlling the photochemical [1,3]- and [1,2]-acyl shifts in but-3-enal are not simple surface crossings or excited state intermediates. In fact, structures **A** and **D** correspond to regions of the potential energy surface where there are *four* degenerate states including two singlets (S_0 and ^{1}(nπ*)) and two triplets (^{3}(nπ*) and ^{3}($\pi\pi$*)). Consequently, these structures can promote decay to the ground state via both internal conversion and intersystem crossing such that the outcome of any photochemical process involving them must be controlled by a subtle mixture of nonadiabatic and dynamic factors. The lack of selectivity of direct versus sensitized irradiation, the sensitivity of the reaction outcome to substituents, and the degree of stereospecificity are therefore related to the character of these decay regions. The alternative is a fragmentation−recombination process via the radical pair **C**, which involves dissociation into a doublet formyl radical and a doublet propenyl radical. The ^{1}(nπ*) fragmentation path leads to an excited state doublet formyl radical which can decay to the ground state at a linear geometry via efficient internal conversion. The ^{3}(nπ*) fragmentation path, which can be populated by ISC from the singlet nπ* surface, just leads to two ground state doublet radicals which are triplet coupled.

The biradical structures **A** and **D** (see Scheme 2) also correspond to intermediates on the ground state surface such that the ground state evolution is independent of the spin multiplicity and the electronic nature (nπ* or $\pi\pi$*) of the excited state that is initially populated. The photoproduct distribution will therefore be determined by the relative barrier heights on the excited state branch of the reaction coordinate which control the accessibility of the different decay regions. Our calculations indicate that the differences between these barriers is small, so that the reaction mechanism in real molecular systems will be controlled by small steric effects on the transition states that separate the decay region from the Franck−Condon region. The existence of the "floppy" intermediates **A** and **B** accounts for the loss in stereochemistry that is usually observed in the ODPM reaction, while the "tightness" of the intermediate **D** explains the stereospecificity of the quasi-concerted [1,3]-acyl shift.

The fluorescence lifetimes recorded showed that on direct photolysis two different mechanisms leading to the [1,3]-acyl shift exist. We have confirmed that these are a dissociation−recombination pathway (which predominates) and a quasi-concerted stereospecific pathway. The CIDNP experiments showed a change on polarization of the radical pairs with temperature: low temperatures yielded triplet radicals while high temperatures yielded singlet radicals. This is in agreement with our results that show the barrier to triplet dissociation is much lower than that leading to singlet fragmentation. The triplet nπ* surface can be populated by ISC from the singlet nπ* surface in the region of the transition states where the C−O π bond is broken since the two nπ* surfaces are very similar in topology and the spin−orbit coupling is about 21 cm^{-1}.

In synthetic work it is usually assumed that direct photolysis generally yields the [1,3]-acyl shift product via the ^{1}(nπ*) state, while the ODPM product arises from population of the ^{3}($\pi\pi$*) state on triplet sensitization. The ^{3}($\pi\pi$*) ODPM rearrangement and the ^{3}($\pi\pi$*) [1,3]-acyl shift reaction both correspond to mechanisms involving ISC at a crossing region (**A** and **D**, respectively), although the difference in barrier heights is only 2 kcal mol^{-1} in favor of the ODPM reaction. In the case of the nπ* [1,3]-acyl shift reactions, the transition structures for dissociation and recombination on the singlet and triplet nπ* surfaces lie about 20 kcal mol^{-1} lower in energy than the transition states leading to the stereospecific [1,3]-acyl shift decay region, such that dissociation and recombination will predominate for acyclic enones. Furthermore, the transition state leading to dissociation on the singlet nπ* surface lies 2 kcal mol^{-1} below the transition state for the ODPM path. This is consistent with the fact that on direct photolysis acyclic enones give exclusively the [1,3]-acyl shift product via dissociation and recombination. However, in other cases both steric and dynamic effects could change the order of these barriers such that both the ODPM reaction and the stereospecific [1,3]-acyl shift reaction could also occur on direct photolysis.

Our work has involved only a "model" system. The main conclusions relate to the topology (i.e., the existence of minima, transition states, and reaction paths), and while this will be well represented at the MC-SCF/6-31G* level, the computed barrier heights will certainly be sensitive to the treatment of dynamic electron correlation. The computed topological features on the potential surface for the model β,γ-enone investigated here must also be present in substituted and cyclic β,γ-enone systems; however, the heights and relative ordering of these barriers will vary according to the molecule photolyzed. These barriers will determine exactly what happens on direct and triplet-sensitized photolysis of these compounds.

Acknowledgment. This research has been supported in part by the SERC (U.K.) under Grant Numbers GR/J25123 and GR/H58070. S.W. is grateful to the SERC for a studentship. All ab-initio computations were run on an IBM RS/6000 using a development version of the Gaussian program.[32]

Supporting Information Available: Tables showing the energetics for reactions from the ^{1}(nπ*), ^{3}($\pi\pi$*), and ^{3}(nπ*) surfaces with energies in hartrees (5 pages). This material is contained in many libraries on microfiche, immediately follows this article in the microfilm version of the journal, can be ordered from the ACS, and can be downloaded from the Internet; see any current masthead page for ordering information and Internet access instructions.

JA9522802